Tapered Glass-Fiber Microspike: High-Q Flexural Wave Resonator and Optically Driven Knudsen Pump

Riccardo Pennetta, Shangran Xie,* and Philip St.J. Russell
Max Planck Institute for the Science of Light, Staudtstrasse 2, 91058 Erlangen, Germany
(Received 21 September 2016; published 29 December 2016)

Appropriately designed optomechanical devices are ideal for making ultra-sensitive measurements. Here we report a fused-silica microspike that supports a flexural resonance with a quality factor greater than 100 000 at room temperature in vacuum. Fashioned by tapering single-mode fiber (SMF), it is designed so that the core-guided optical mode in the SMF evolves adiabatically into the fundamental mode of the air-glass waveguide at the tip. The very narrow mechanical linewidth (20 mHz) makes it possible to measure extremely small changes in resonant frequency. In a vacuum chamber at low pressure, the weak optical absorption of the glass is sufficient to create a temperature gradient along the microspike, which causes it to act as a microscopic Knudsen pump, driving a flow of gas molecules towards the tip where the temperature is highest. The result is a circulating molecular flow within the chamber. Momentum exchange between the vibrating microspike and the flowing molecules causes an additional restoring force that can be measured as a tiny shift in the resonant frequency. The effect is strongest when the mean free path of the gas molecules is comparable with the dimensions of the vacuum chamber. The system offers a novel means of monitoring the behavior of weakly absorbing optomechanical sensors operating in vacuum.

DOI: 10.1103/PhysRevLett.117.273901

The ability to read out the mechanical motion of high-Q mechanical resonators optically makes them ideal for high-precision measurements at micrometer and nanometer length scales, offering major advantages for both fundamental studies and applications [1]. Several such systems have been introduced for measuring physical quantities such as displacement [2], force [3], electric field [4], magnetic torque [5], and temperature [6]. Recently, there have been reports of ultra-low-noise clamped Si_3N_4 membrane systems that pave the way to sensitive quantum measurements at room temperature [7,8].

A narrow mechanical linewidth is essential for ultrahigh sensitivity and precision [9]. To achieve this, most experiments are carried out at low pressure so as to avoid gas-related viscous damping and provide better isolation from environmental disturbance. The lack of convective or conductive heat dissipation in the gas at low pressure, together with the relative inefficiency of radiative heat loss, means that even a very small amount of optical absorption can result in a large rise in temperature, even reaching the melting point of fused silica [6,10].

For moderate thermal heating, it might at first be thought that the smaller temperature increase will have little if any effect. In this Letter we report, however, that even a moderate amount of heating can noticeably affect the mechanical behavior of a fused silica microspike resonator. The microspikes were fabricated by scanning an oxybutane flame along a single-mode fiber (SMF) while gently pulling it. They offer low-loss, single-mode optical guidance and a mechanical linewidth of a few tens of mHz for the fundamental flexural mode, corresponding to a Q factor greater than 10^5. Our results show that a significant optothermal "Knudsen stiffness" can act on the microspike if the temperature distribution along it is nonuniform. A temperature gradient as small as several K/mm is sufficient to shift the resonant frequency by ~0.03% (resolvable because the Q is so high) as a consequence of the interaction between the microspike and the collective motion of the gas molecules. This effect is strongest in the Knudsen regime, when the mean free path of the air molecules is comparable to the dimensions of the vacuum chamber.

By adjusting the pulling speed and the flame temperature, a wide range of different taper profiles could be produced. The experimental results presented here were obtained using the microspike in Fig. 1(a). The taper is ~4.3 mm long with a tip diameter of ~3.9 μm, and optical adiabaticity was guaranteed by ensuring that the taper profile followed the length-scale criterion [11] (see Supplemental Material [12]). The microspike was placed in a vacuum chamber and laser light launched into the untapered end of the SMF. The mechanical displacement of the microtip was monitored using a telescope to couple the emitted light into a second length of SMF [Fig. 1(b)]. The transmitted signal was monitored using a balanced photodiode to suppress laser noise, and was found to be linearly dependent on tip displacement (see Supplemental Material [12]).

Figure 1(c) plots the Brownian motion spectrum recorded at 10^{-5} mbar and 300 K for frequencies close to the fundamental flexural resonance of the microtip. The resonant frequency is $\Omega/2\pi \approx 4340$ Hz, in good agreement with the value of 4338 Hz predicted by finite element modeling

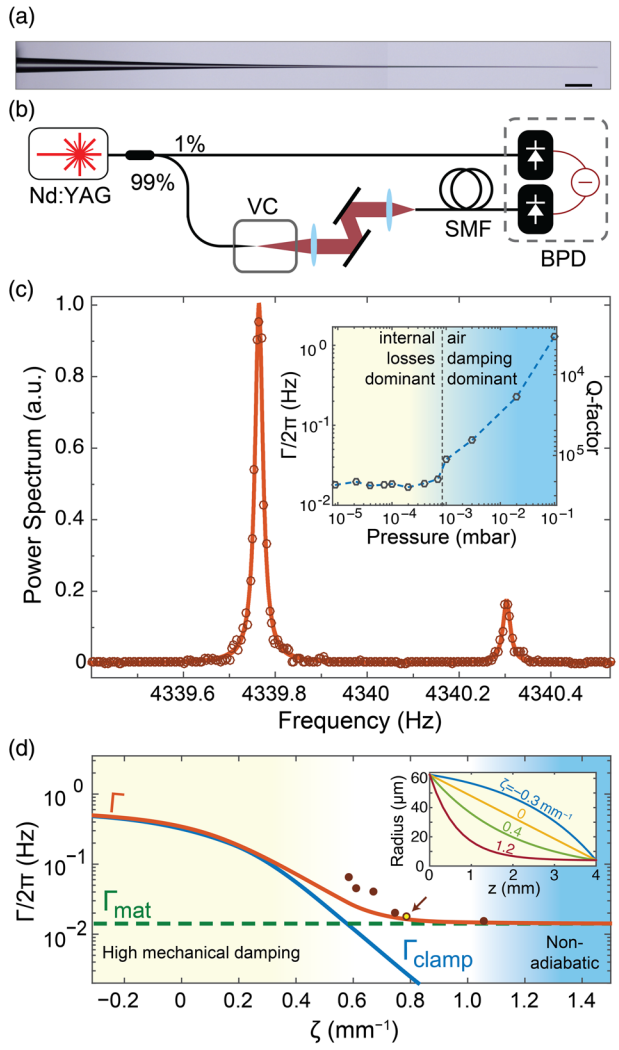

FIG. 1. (a) Optical micrograph of the microspike (scale bar = 200 μm). (b) Schematic of the experimental setup, including a vacuum chamber (VC), SMF, and a balanced photodiode (BPD). (c) Mechanical power spectrum of the microspike driven by Brownian motion. (d) Finite-element modeling of clamping loss of the microspike as a function of taper profile. The dots are measured data points, and the arrow marks the parameters of the microspike used in the experiments. See text for more details.

(FEM). The measured linewidth is $\Gamma/2\pi = 20$ mHz, corresponding to a resonance lifetime $\tau = 50$ s and a Q factor of $\Omega/\Gamma = 217\,000$. This ultranarrow linewidth makes it possible to distinguish two peaks only 0.6 Hz apart in the spectrum. We attribute this frequency difference, which was independent of laser power and gas pressure, to a noncircular microspike cross section, resulting in a small splitting of the resonant frequency between orthogonal modes. The inset in Fig. 1(c) plots the mechanical linewidth as a function of gas pressure. Above $\sim 10^{-3}$ mbar it is dominated by air-related viscous damping and at lower pressures it saturates to 20 mHz, a value determined by material and clamping losses.

The total phonon decay rate Γ can be expressed as the sum $\Gamma_{\mathrm{mat}} + \Gamma_{\mathrm{clamp}} + \Gamma_{\mathrm{air}}$, where Γ_{mat} is caused by material losses (friction) in the glass, Γ_{clamp} by leakage into the supporting fiber, and Γ_{air} by viscous damping in the air. Since tailoring the geometry of the microspike can reduce clamping loss, FEM of the mechanical modes of a clamped microspike was performed in order to understand the dependence of clamping loss on the taper profile. Different microspike shapes were modeled using the following expression for the radius:

$$R(z) = \frac{R_0(e^{-\zeta L} - e^{-\zeta z}) + R_T(e^{-\zeta z} - 1)}{e^{-\zeta L} - 1}, \qquad (1)$$

which runs from $z = 0$ ($R = R_0$, the untapered fiber radius) to $z = L$ ($R = R_T$, at the tip) where ζ is a shape constant (when $\zeta = 0$ the profile is linear). The inset in Fig. 1(d) shows $R(z)$ for different values of ζ, while Fig. 1(d) plots the corresponding simulated clamping losses. In the same plot, material losses were introduced to reproduce the saturation in the total losses observed in the experiment; the results are consistent with reported values [16]. It can be seen that the clamping losses decrease strongly as ζ increases (i.e., for sharper taper profiles) because of better confinement of phonons within the spike, while for ζ greater than ~ 0.6 mm^{-1} material losses dominate. Since the microspike is optically nonadiabatic for ζ greater than ~ 1.2 mm^{-1} (the light-blue shaded area), there is a well-defined window within which minimum mechanical damping can be reached without affecting the optical properties of the microspike—the experiment reported here lies within this region [marked with an arrow in Fig. 1(d)].

The ultranarrow mechanical linewidth of the microspike makes it ideal for probing weak physical processes in vacuum. The pressure-dependent behavior of gases is normally characterized by the Knudsen number (Kn), defined as the ratio between the mean free path and a characteristic length (in our case the width of the vacuum chamber, $L = 2$ cm). In the experiments we worked in the range $0.01 < \mathrm{Kn} < 1000$. For large values of Kn we enter the free-molecular regime, when gas dynamics is dominated by collisions with the constraining chamber rather than intermolecular collisions as in the continuum (high pressure) regime. Figure 2(a) plots the measured resonant frequency f_R of the microspike as a function of gas pressure for different values of laser power. The corresponding value of Kn is given along the upper axis for reference. The results show that f_R first increases and then decreases with pressure, reaching a maximum at around 10^{-3} mbar when $\mathrm{Kn} \sim 1$. This nonmonotonic behavior becomes more pronounced at higher laser power. At fixed gas pressure, f_R is found to be a linear function of laser power (see Supplemental Material [19]). This is in sharp contrast to the behavior predicted by gaseous damping [17,18] and thermal effects [19], when f_R increases

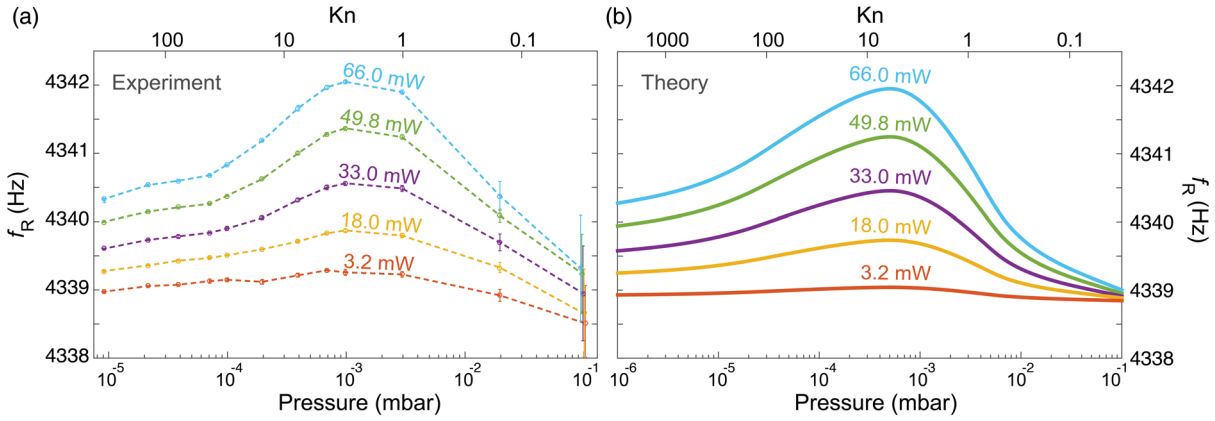

FIG. 2. (a) Measured and (b) simulated mechanical resonant frequency of the microspike as a function of gas pressure for five different laser powers.

monotonically as the pressure is lowered. In particular, gaseous damping is independent of laser power and is, anyway, negligible in the regime studied here. For the microspike, thermal effects are driven by the increase in the Young's modulus of silica with temperature [19], which makes the microspike stiffer and raises f_R. As expected, simulations of the heat dissipation processes show that the average temperature of the microspike (and, thus, the thermal frequency shift) increases monotonically as the pressure is reduced [see Fig. 3(a)].

To fully understand the physical mechanisms behind this anomalous pressure dependence of f_R, FEM was used to simulate the interaction between the microspike and the gas molecules, by solving the Navier-Stokes equations with slip boundary conditions [20]. Figure 3(a) plots the temperature distribution along the microspike at various gas pressures, using the absorption of thermally treated silica fiber (see Supplemental Material [20]). It can be seen that the expected average temperature rise is accompanied by a highly nonuniform temperature distribution along the microspike (z axis), reaching a maximum at the tip. This temperature gradient drives the gas molecules along the surface of the microspike towards higher temperature, creating a collective gas flow in the vacuum chamber within a layer of thickness comparable to the mean free path. Known as thermal creep flow [21], this effect has been recognized as the cause behind the singular behavior of Crookes radiometers and is the mechanism behind Knudsen pumps [22,23]. Most recently it has been used to create an optothermal particle trap in gas-filled hollow-core photonic crystal fibers [24].

The calculated flow pattern at 10^{-3} mbar (Kn ~ 1) is plotted in Fig. 3(b), where the black solid curves represent the average trajectories of the gas molecules (the streamlines) and the red arrows mark the local velocity directions. The mean molecular velocity can reach some m/s in the vicinity of the microspike [inset of Fig. 3(b)]. Using the temperature gradient calculated by FEM, this average velocity along the gas-solid surface can also be analytically calculated using the formula proposed by Maxwell [25,26],

$$v_{\text{creep}} = \frac{3}{4}\frac{\eta}{\rho T}\frac{\partial T}{\partial z}, \tag{2}$$

where η is the gas viscosity, ρ is the density, and T is the temperature. The inset in Fig. 3(a) plots v_{creep} versus pressure at $z = 4$ mm on the microspike surface, showing excellent agreement between Eq. (2) and the results of full-FEM simulations.

Although it is also possible to excite a gas flow when the temperature distribution is uniform, this only occurs if the solid-gas interface has points where the curvature changes sharply, creating thermal edge flow [27,28]. For pressures below 10^{-3} mbar, however, simulations show that thermal creep flow dominates over thermal edge flow in the microspike (see Supplemental Material [12]).

The microspike stiffness changes as a result of its interaction with the gas flow. When it moves away from its equilibrium position, it causes a local perturbation in the gas flow. Molecules are deflected from their trajectories, resulting in transfer of momentum to the microspike. Since the molecules flow towards the tip of the microspike, this creates a restoring force that pushes the microspike back towards its equilibrium position. Figure 3(c) plots the calculated Knudsen force per unit length F_{Kn} along the microspike for a maximum deflection of 1 μm (blue curve) and a launched power of 66 mW. For small tip deflections, calculations predict that this restoring force is proportional to the displacement and, thus, effectively increases f_R. In the simulations the gas was once again modeled using the Navier-Stokes equations.

The purple dash-dotted curve in Fig. 4 plots the resulting Knudsen stiffness, calculated by FEM, against gas pressure, and reproduces the typical trend seen in the experiments. Intuitively, it is clear that, at higher pressure, efficient thermal dissipation through the surrounding air

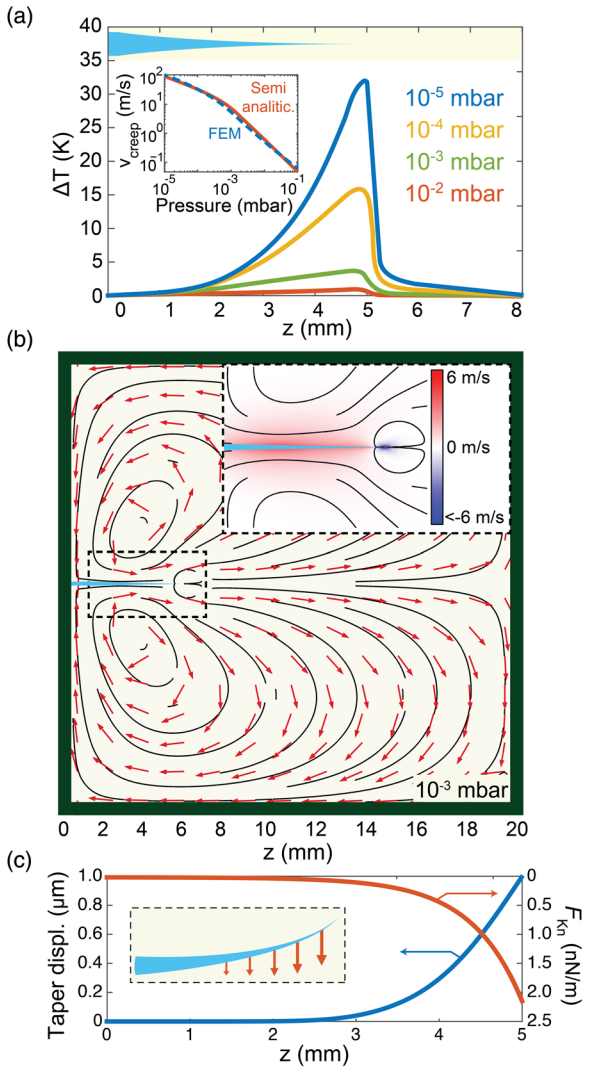

FIG. 3. Numerical simulations of the microspike-driven Knudsen flow. (a) Temperature gradient along the microspike at different gas pressures. Inset: velocity of thermal creep flow at the surface of the microspike at $z = 4$ mm. The orange line plots Eq. (1), while the blue dashed line is the result of FEM simulations. (b) Numerically simulated Knudsen flow inside the chamber at 10^{-3} mbar. The black solid curves represent the trajectories of the gas molecules (the flow) and the red arrows show the average direction of the molecular velocity. Inset: zoom-in of the region close to the tip. (c) Simulations of the additional restoring force per unit length F_{Kn} calculated for a maximum tip deflection of 1 μm and 66 mW input power.

will suppress the temperature gradient and slow the gas flow, while at low pressure the temperature gradient will saturate while the molecular density (and thus the momentum transfer) falls. Overall this will result in maximum Knudsen stiffness at $\mathrm{Kn} \sim 1$, as seen in the experiments.

Since the resonant frequency is proportional to the square root of the stiffness, small additions δk to the stiffness k_0 will increase the frequency, to a good approximation, by an amount equal to $f_R \delta k/(2k_0)$. We can

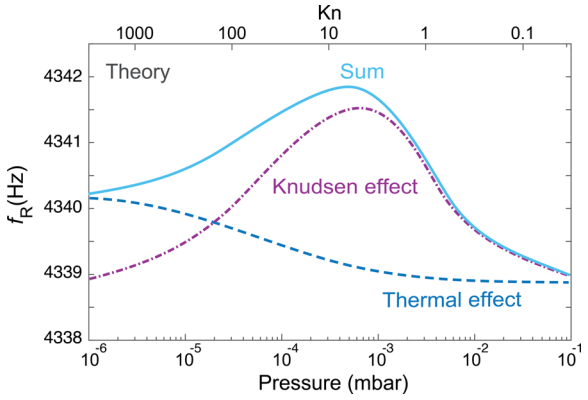

FIG. 4. Contributions from pure thermal (dark-blue dashed line) and Knudsen (purple dotted line) effects to the resonant frequency of the microspike as a function of gas pressure. The solid blue curve is the sum of two effects.

therefore write $f_R = f_0 + \Delta f_{\mathrm{th}} + \Delta f_{\mathrm{Kn}}$, where f_0 is the resonant frequency at room temperature in vacuum, Δf_{th} results from the temperature dependence of Young's modulus, and Δf_{th} is the Knudsen contribution.

The simulated overall frequency shift for a launched power of 66 mW is plotted in Fig. 4 (solid blue curve) as the sum of Δf_{th} and Δf_{Kn}. The frequency shift is small compared to f_0 and is proportional to the optical power, as measured in the experiments. As shown in Fig. 2(b), the simulations reproduce the observed behavior very well at several different power levels. Quantitatively, the predicted and measured frequency shifts agree well, while the gas pressure at which the Knudsen effect reaches a maximum is somewhat higher in the experiment (Fig. 2). We attribute this discrepancy to the fact that the Navier-Stokes equations are not precisely correct in the free molecular regime ($\mathrm{Kn} > 10$).

To further test the validity of this physical picture, the microspike was gradually inserted axially into a glass capillary with an inner diameter of 100 μm, so as to perturb the gas flow around the microspike [see inset in Fig. 5(a)]. The mechanical motion of the microspike was captured by collecting the light emerging from the capillary using a quadrant photodiode (QPD). The measured f_R falls as the insertion length L_{ins} is increased from -0.5 to 0.3 mm [Fig. 5(a)], where positive values of L_{ins} mean that the microspike was actually inserted in the capillary. The measurement was performed at a pressure of 10^{-3} mbar, when the Knudsen stiffness is maximum (note that in this configuration the optomechanical trapping force reported in [29] is negligible, due to almost complete confinement of optical mode inside the microspike and the large inner diameter of the capillary). As a consequence, the drop in f_R can only be caused by a change in the molecular flow around the tip, because the capillary does not physically or optically interact with the microspike. The simulation in Fig. 5(b) shows the disruption to the streamlines of gas flow, resulting in suppression of the Knudsen effect.

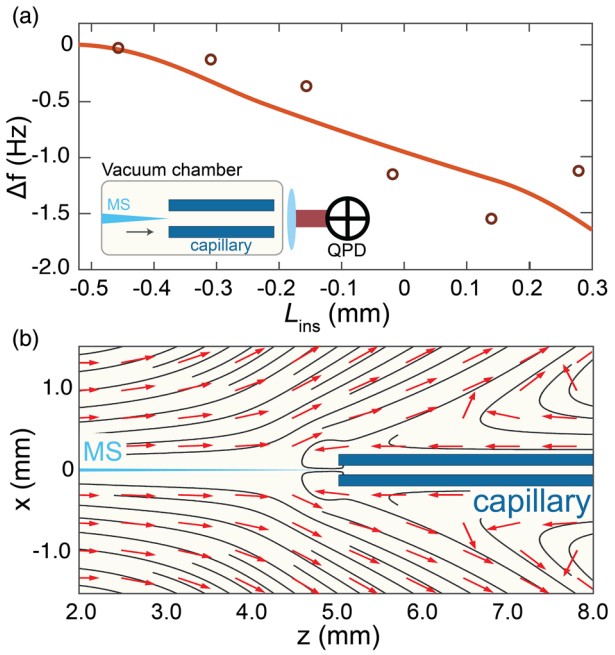

FIG. 5. (a) Frequency shift as a function of insertion length L_{ins} in a glass capillary with internal diameter 100 μm. Inset: sketch of the experimental setup. The circles are experimental data points and the full orange line is the numerical simulation. (b) Simulated gas flow around the microspike at $L_{ins} = 0$. The black solid lines plot the trajectories of the gas molecules.

In conclusion, silica microspikes formed from suitably tapered single-mode fibers support high-Q flexural resonances and are optically adiabatic. They provide a highly sensitive and convenient probe of optothermal and optomechanical effects at low gas pressures, for example, molecular pumps based on the Knudsen effect. The novel system may be useful for understanding the behavior of laser tweezered particles under vacuum conditions when residual absorption can create temperature gradients. The microspike also seems naturally suited to optical near-field measurements and, if coated with metals, could also be used to sense electric and magnetic fields.

We thank R. E. Noskov, T. G. Euser, and D. S. Bykov for useful discussions.

*shangran.xie@mpl.mpg.de

[1] M. Aspelmeyer, T. J. Kippenberg, and F. Marquardt, Rev. Mod. Phys. **86**, 1391 (2014).
[2] M. R. Vanner, J. Hofer, G. D. Cole, and M. Aspelmeyer, Nat. Commun. **4**, 2295 (2013).
[3] G. Ranjit, D. P. Atherton, J. H. Stutz, M. Cunningham, and A. A. Geraci, Phys. Rev. A **91**, 051805 (2015).
[4] D. S. Bykov, O. A. Schmidt, T. G. Euser, and P. St. J. Russell, Nat. Photonics **9**, 461 (2015).
[5] M. Wu, N. L. Wu, T. Firdous, F. F. Sani, J. Losby, M. Freeman, and P. Barclay, in *Conference on Lasers and Electro-Optics*, OSA Technical Digest (Optical Society of America, Washington, DC, 2016), paper STu4E.1.
[6] J. Millen, T. Deesuwan, P. Barker, and J. Anders, Nat. Nanotechnol. **9**, 425 (2014).
[7] C. Reinhardt, T. Muller, A. Bourassa, and J. C. Sankey, Phys. Rev. X **6**, 021001 (2016).
[8] R. A. Norte, J. P. Moura, and S. Groblacher, Phys. Rev. Lett. **116**, 147202 (2016).
[9] P. R. Saulson, Phys. Rev. D **42**, 2437 (1990).
[10] A. Rahman, A. C. Frangeskou, M. S. Kim, S. Bose, G. W. Morley, and P. F. Barker, Sci. Rep. **6**, 21633 (2016).
[11] J. D. Love, W. M. Henry, W. J. Stewart, R. J. Black, S. Lacroix, and F. Gonthier, IEE Proceedings J, Optoelectronics (1985-1993) / IEE Proc-J: Optoelectronics **138**, 343 (1991).
[12] See Supplemental Material at http://link.aps.org/supplemental/10.1103/PhysRevLett.117.273901, for additional details regarding the experimental setup and the methodology adopted in the numerical simulations, which includes Refs. [13–15].
[13] A. Trowbridge, Phys. Rev. **2**, 58 (1913).
[14] E. M. Lifschitz and L. P. Pitajewski, *Textbook of Theoretical Physics* (Elsevier, Oxford, UK, 1983), Vol. 10.
[15] D. K. Hutchins, M. H. Harper, and R. L. Felder, Aerosol Sci. Technol. **22**, 202 (1995).
[16] D. B. Fraser, J. Appl. Phys. **41**, 6 (1970).
[17] M. Christen, Sens. Actuators **4**, 555 (1983).
[18] K. Kokubun, M. Hirata, M. Ono, H. Murakami, and Y. Toda, J. Vac. Sci. Technol. A **3**, 2184 (1985).
[19] S. Spinner, J. Am. Ceram. Soc. **39**, 113 (1956).
[20] E. Davis and G. Schweiger, *The Airborne Microparticle* (Springer-Verlag, Berlin, 2002).
[21] B. K. Annis, J. Chem. Phys. **57**, 2898 (1972).
[22] M. Knudsen, Ann. Phys. (Berlin) **333**, 75 (1909).
[23] S. E. Vargo, E. P. Muntz, G. R. Shiflett, and W. C. Tang, J. Vac. Sci. Technol. A **17**, 2308 (1999).
[24] O. A. Schmidt, M. K. Garbos, T. G. Euser, and P. St. J. Russell, Phys. Rev. Lett. **109**, 024502 (2012).
[25] J. C. Maxwell, Phil. Trans. R. Soc. London **170**, 231 (1879).
[26] D. A. Lockerby, J. M. Reese, D. R. Emerson, and R. W. Barber, Phys. Rev. E **70**, 017303 (2004).
[27] A. Passian, R. J. Warmack, T. L. Ferrell, and T. Thundat, Phys. Rev. Lett. **90**, 124503 (2003).
[28] T. S. Zhu and W. J. Ye, Phys. Rev. E **82**, 036308 (2010).
[29] S. Xie, R. Pennetta, and P. St. J. Russell, Optica **3**, 277 (2016).